

Metrology and multipartite entanglement in measurement-induced phase transition

Giovanni Di Fresco,^{1,*} Bernardo Spagnolo,^{1,†} Davide Valenti,^{1,‡} and Angelo Carollo^{1,§}

¹*Dipartimento di Fisica e Chimica “Emilio Segrè”,
Group of Interdisciplinary Theoretical Physics, Università degli studi di Palermo,
Viale delle Scienze, Ed. 18, I-90128 Palermo, Italy*

Measurement-induced phase transition arises from the competition between a deterministic quantum evolution and a repeated measurement process. We explore the measurement-induced phase transition through the quantum Fisher information in two different metrological scenarios. We demonstrate through the scaling behavior of the quantum Fisher information the transition of the multi-partite entanglement across the phases. In analogy with standard quantum phase transition, we reveal signature of a measurement-induced phase transition in the non-analytic behaviour of the quantum Fisher information as the measurement strength approaches the critical value. Our results offer novel insights into the features of a quantum systems undergoing measurement-induced phase transition and indicate potential avenues for further exploration in the field of quantum physics.

A many-body quantum system subject to a measurement process may undergo abrupt changes, similar to quantum phase transitions (QPTs), as a function of the monitoring rate [1–7]. Unlike conventional QPT that are driven by external factors, these criticalities, called measurement-induced phase transition (MIPT), arise from the interplay between the deterministic unitary evolution and the measurement process. This phenomenon has been found to have important implications for understanding the properties of many-body quantum systems, such as the onset of quantum entanglement [8–14] and the emergence of topological order [15].

In this letter we propose to explore the concept of MIPT through the use of QFI. The reason to characterise this phenomenon through QFI is two-fold. On the one hand, the QFI is a measure of the sensitivity of a quantum system to small changes in a parameter. As such, the QFI has been widely exploited to signal and characterise the critical behaviour of equilibrium [16–29] as well as non-equilibrium QPTs [30]. It is thus natural to ask whether and how the QFI may respond to critical transitions when the latter are driven by measuring processes. On the other hand, one of the characterising features of MIPT is an observable qualitative change of the system’s entanglement properties, which has been observed through the scaling behavior of the entanglement entropy [1–6]. The QFI is a witness of multi-partite entanglement [31–34], as well known from quantum metrology [35–49]. It thus provides a complementary characterisation of quantum correlation across MIPT, beyond entanglement entropy: on the one hand QFI reveals the multi-partite nature of entanglement, on the other it distinguishes metrologically useful quantum correlation from other forms of entanglements. Moreover, QFI provides a means to characterize entanglement of systems which are not necessarily pure states, a technical limitation which affects other measures, such as the entanglement entropy.

Motivated by the above arguments, we examine the QFI in two complementary metrological scenarios. In both

of them we consider as a prototypical example the MIPT of a one-dimensional Ising chain in a transverse field and subject to a continuous observation. In the first scenario, we investigate the QFI associate to the system’s response to a single-parameter unitary transformation. This metrological scheme, is the standard scenario in which the scaling of QFI can be used as a witness of multipartite entanglement. In the second scenario, we study the time-dependent behavior of the QFI after the system undergoes a quench in the monitoring rate. Our analysis uncovers an exponential scaling of the QFI, where we identify a non-analyticity of the QFI when the measurement strength approaches the critical value. Our findings provide new insights into the behavior of quantum systems subjected to MIPT, and the role of the QFI in characterizing the associated quantum criticality.

Model— We consider a one-dimensional Ising chain with a transverse magnetic field [50–52]

$$H = - \sum_i [\sigma_i^x \sigma_{i+1}^x + h \sigma_i^z] \quad (1)$$

which is coupled to an apparatus that measures $n = \frac{1+\sigma_z}{2}$, with γ as a coupling, such that the evolution of the system is given by the stochastic quantum jump differential equation [5]

$$d|\psi\rangle = -iHdt|\psi\rangle - \frac{\gamma}{2}dt \sum_i (n_i - \langle n_i \rangle_t) |\psi_t\rangle + \sum_i dN_t^i \left(\frac{n_i}{\sqrt{\langle n_i \rangle_t}} - 1 \right) |\psi\rangle. \quad (2)$$

The variable dN_t^i is a stochastic Poisson variable ($dN_t^i = 0, 1$), with each noise source being delta-correlated and ensemble average $\overline{dN_t^i} = \gamma \langle n_i \rangle_t dt$. In this paper, however, we are interested in trajectories in which no jump occurs (no-click limit), which corresponds to a deterministic post-selected dynamics fixed by the non-Hermitian Hamiltonian

$$H_{\text{eff}} = H - \frac{i\gamma}{2} \sum_i n_i. \quad (3)$$

The system has a critical point at $\gamma_c = 4\sqrt{1-h^2}$ [4, 6, 53], that marks two regions in which the entanglement goes from a logarithmic scaling to a constant scaling in the system size [5, 6].

The model can be diagonalized in the fermionic formalism as [6, 53]

$$H = \sum_k \begin{pmatrix} c_k^\dagger & c_{-k} \end{pmatrix} M_k \begin{pmatrix} c_k \\ c_{-k}^\dagger \end{pmatrix} \quad (4)$$

where

$$M_k = \begin{pmatrix} \alpha_k & \beta_k \\ \beta_k & -\alpha_k \end{pmatrix} \quad (5)$$

and $\alpha_k = -2\cos k - 2h - \frac{i\gamma}{2}$, $\beta_k = 2\sin k$. The eigenvalues of Eq. (5), $\epsilon_k = \pm\sqrt{\alpha_k^2 + \beta_k^2}$, have both real and imaginary part, which we denote as $E_k = \Re(\epsilon_k)$ and $\Gamma_k = \Im(\epsilon_k)$. We choose as our ground state for each k the value with negative imaginary part [53]. The spectrum has a critical mode for $k = \arccos(-h)$ whose eigenvalue is real for $\gamma < \gamma_c$ and imaginary for $\gamma > \gamma_c$.

Entanglement properties— This section aims to show that the scaling properties of QFI can also be used to detect the entanglement properties of MIPT. To achieve this goal, we follow the procedure outlined in Ref. [5] to compute the time evolution of our system. It is worth noting that due to the system's quadratic nature at all times, the ground state can be expressed as

$$|\psi\rangle(t) = \frac{1}{\sqrt{\det(U)}} \exp\left(\frac{1}{2} \sum_{j_1 j_2} Z_{j_1 j_2} c_{j_1}^\dagger c_{j_2}^\dagger\right) |0\rangle, \quad (6)$$

where $Z = -(U^\dagger)^{-1} V^\dagger$. U and V are the elements of the 2×2 matrix

$$\mathcal{U}_t = \begin{pmatrix} U_t & V_t^\dagger \\ V_t & U_t^\dagger \end{pmatrix}. \quad (7)$$

This matrix is the rotation matrix that transforms our original fermionic operators (c_i, c_j^\dagger) to a new set (χ_i, χ_j^\dagger)

$$\begin{pmatrix} \chi \\ \chi^\dagger \end{pmatrix} = \mathcal{U}_t \begin{pmatrix} c \\ c^\dagger \end{pmatrix} \quad (8)$$

such that $\chi_i |0\rangle = 0 \forall i$. The dynamics of the system is all encoded in the operator \mathcal{U} and its Heisenberg equation of motion is [5]

$$d\mathcal{U} = (-iH_{\text{eff}} dt) \mathcal{U}. \quad (9)$$

To utilize QFI as an entanglement witness, meticulous preparation of the metrology scheme is needed [34]. Specifically, we opt for open boundary conditions, and set $h = 0$ in Eq. (1). This choice is made because the presence of a transverse magnetic field does not affect

deeply the aspects of our interest. Moreover, for the simpler quantum Ising chain, selecting the appropriate generator of the unitary transformation is more straightforward. After initiating the state evolution in accordance with Eq.(9), we introduce the estimation parameter via unitary evolution at time t

$$\rho_\varphi = e^{-i\varphi S_x} \rho(t) e^{i\varphi S_x}, \quad (10)$$

where S_x is the spin operator [54]. The QFI associated to Eq. (10) is [55]

$$F = 4\Delta^2(S_x). \quad (11)$$

where $\Delta^2 S_x$ is the variance of the spin operator (we follow the results of Ref. [51] to evaluate this quantity). Fig. 1 shows the scaling of the QFI in the two different phases of the system. Specifically, panel (b) of the figure depicts the scaling of the QFI for $\gamma < \gamma_c$, which exhibits a super extensive dependence on the system size N ($F_Q \propto N^\eta$) with $\eta > 1$ (e.g., $\eta = 1.5$ in the illustrated case). In contrast, panel (a) shows that for $\gamma > \gamma_c$, the QFI follows a normal scaling behavior with $\eta = 1$. These distinct scaling behaviors not only enable QFI to serve as a valuable metric for characterizing MIPT, but also offer a means to identify the presence of multipartite entanglement in the state, which is beyond the scope of the entanglement entropy. Indeed, it is well known that if

$$\frac{F}{N} \leq m, \quad (12)$$

in the system there is at least a $(m+1)$ -partite entanglement [31–34].

Non-Hermitian quantum quench— This section aims to investigate the QFI of a system initially prepared in the ground state of the unperturbed Ising Hamiltonian and quenched at time t by the application of the continuous measurement process, leading to the deterministic non-Hermitian Hamiltonian evolution H_{eff} . Our goal is to demonstrate that the effect of MIPT on the QFI is similar to that of a second order QPT (i.e., a divergence at the critical point). To this end, we select the ground state of Eq. (1) as initial state with periodic boundary conditions, which allows us to use the Hamiltonian expression in k -space. The final state can be expressed in a general form

$$|\psi_t\rangle = N(t) e^{-iH_{\text{eff}} t} |\psi_0\rangle, \quad (13)$$

where $N(t)$ is a normalization factor. To compute the QFI for the state in Eq. (13), it is necessary to extend the results of Ref. [56] for a non-Hermitian Hamiltonian. The QFI can be evaluated using the expression

$$F = 4 \left(\langle \partial_\lambda \psi | \partial_\lambda \psi \rangle - |\langle \partial_\lambda \psi | \psi \rangle|^2 \right). \quad (14)$$

We found that in a non-Hermitian scenario the QFI will depend on the covariance of the operator O_λ (the detailed

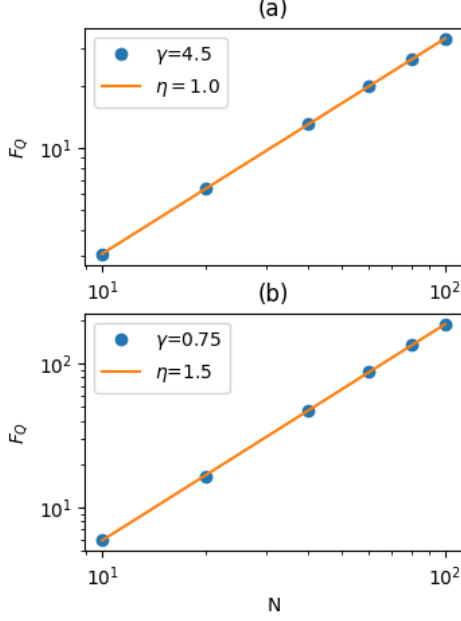


FIG. 1. The scaling behavior of the QFI is presented in these log-log plots, with $x = 1$ and $h = 0$ in both panels: (a) for $\gamma = 4.5$ the system is in a phase where the entanglement remains constant with respect to the system size, resulting in a linear scaling of the QFI; (b) for $\gamma = 0.75$ the system is in a phase where the entanglement varies with the system size, leading to an enhanced scaling of the QFI.

derivation is provided in Appendix B)

$$\frac{F}{4} = \langle \psi | O_\lambda^\dagger O_\lambda | \psi \rangle - |\langle \psi | O_\lambda | \psi \rangle|^2, \quad (15)$$

which is defined as

$$O_\lambda = \int_0^t ds \exp(-iH_{\text{eff}}s) \partial_\lambda (-iH_{\text{eff}}) \exp(iH_{\text{eff}}s). \quad (16)$$

If we want to estimate the parameter γ , this expression can be cast as a quadratic function of the fermionic operator c_k and c_k^\dagger in the following closed form

$$O_\gamma = - \sum_k (c_k^\dagger \ c_{-k}) R_k \begin{pmatrix} c_k \\ c_{-k}^\dagger \end{pmatrix} - \frac{Nt}{4}. \quad (17)$$

where R_k is a 2×2 time dependent matrix (see appendix B)

The state at time t [6] can be written as

$$|\psi\rangle = \prod_k \frac{u_k(t) + v_k(t) c_k^\dagger c_{-k}^\dagger}{\sqrt{|u_k|^2 + |v_k|^2}} |0\rangle, \quad (18)$$

where

$$\begin{cases} u_k(t) = u_k(0) \cos(\varepsilon t) - i \left(\frac{\beta}{\varepsilon} v_k(0) - \frac{\alpha}{\varepsilon} u_k(0) \right) \sin(\varepsilon t) \\ v_k(t) = v_k(0) \cos(\varepsilon t) - i \left(\frac{\beta}{\varepsilon} u_k(0) + \frac{\alpha}{\varepsilon} v_k(0) \right) \sin(\varepsilon t). \end{cases} \quad (19)$$

If we now evaluate the expression of the QFI in Eq.(15), after some tedious but straightforward algebra, we end up with Eq. (37) in Appendix B.

The QFI as a function of time is depicted in Fig. 2. It is observed that, following an initial transient period whose duration is dependent on γ , an exponential scaling regime emerges, with a scaling behavior approaching 2γ . The exponential divergence observed is related to the non-Hermiticity of the model and it arises from the imaginary part of the spectrum. It is however not directly related to the critical features of the system.

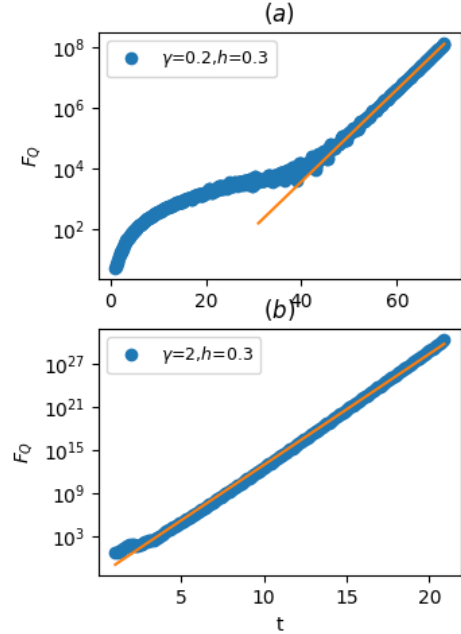


FIG. 2. The figure presents the time evolution of the quantum Fisher information (QFI) for various parameters of the Hamiltonian. In panels (a) and (b) we fix $h = 0.3$. We observe that an exponential scaling emerges, which depends on γ and occurs at a time that varies with the parameter values. Specifically, in panel (a), with $\gamma = 0.2$, the exponential scaling occurs at a time that differs from panel (b), where $\gamma = 2$.

The effects of MIPT on QFI, which can potentially manifest itself in a non-analytic behaviour of QFI across the MIPT, is partially concealed by this exponential time dependence. In order to unveil the singular part of QFI one can suitably factor out the exponential scaling. This procedure provides a smooth mapping which leaves the analytic properties of the QFI unaltered. Indeed, when examining the long-time behavior of the QFI, one can decompose the QFI in terms of the eigenmodes k , each

dominated by a specific time-dependent exponential factor [57]

$$F = \sum_k F_k e^{4\Gamma_k t}. \quad (20)$$

where, we recall, Γ_k 's are the imaginary part of the eigenvalues ϵ_k while F_k 's are time-independent coefficients, which are expressed in detail in appendix B. The Γ_k functions are continuous with respect to γ , hence, any divergences of QFI due to the MIPT are to be found in the F_k terms. Moreover, one can explicitly relate any divergent behaviour of the QFI to that of an auxiliary function $\bar{F} = \sum_k F_k$ thanks to the following chain of inequalities

$$\bar{F} < F < e^{\frac{\Gamma_{\max}}{4} t} \bar{F}, \quad (21)$$

where Γ_{\max} is the maximum value of the imaginary part of the spectrum, which is a continuous function of γ . This shows that \bar{F} retains the same divergent behaviour of F , but its study is considerably more amenable to numerical analysis, due to the absence of the exponential factors $e^{4\Gamma_k t}$. In Fig. 3 we plot the dependence of \bar{F} on γ , which clearly displays a peak at the critical value $\gamma = \gamma_c$, with a distinctive asymmetric behaviour as the criticality is approached from either above or below.

We analytically derive the singular part of the QFI (see Appendix B for details), which scales as

$$F \sim F_{k_c} \propto \begin{cases} (\gamma - \gamma_c)^{-3} & \gamma > \gamma_c \\ (\gamma_c - \gamma)^{-2} & \gamma < \gamma_c, \end{cases} \quad (22)$$

where $k_c = \arccos(-h)$ is a critical mode, i.e. the mode which is gapless at the MIPT. These features are in accordance with the numerical results shown in Fig. 3 and confirm them as a distinctive signature of the MIPT in the QFI behavior. The non-analytical behaviour of QFI is strictly related to the closing of the gap at criticality. In particular, the different scaling laws as the critical point is approached from above or below γ_c can be pinpointed to the different character of the spectrum at the two sides of the criticality. The critical point is in fact an exceptional point [53] of the model. This is associated to a gap of the model which is real for $\gamma < \gamma_c$ and imaginary for $\gamma > \gamma_c$. Heuristically, these qualitatively different behaviours of the spectrum reflect the distinct characters of the two phases: (i) $\gamma < \gamma_c$ in which, as in standard QPT, the dynamics is dominated by coherent phenomena, with a real energy gap, and (ii) $\gamma > \gamma_c$ where the dynamics is driven by measurement processes, entailing a dissipative, Zeno-like gap. In both cases, the divergence of the QFI manages to capture the closing of the gap, and discriminates the distinctive features of the two phases through the asymmetry of scaling laws.

Conclusion— We have studied the impact of the MIPT on the QFI of a one-dimensional Ising chain subjected to

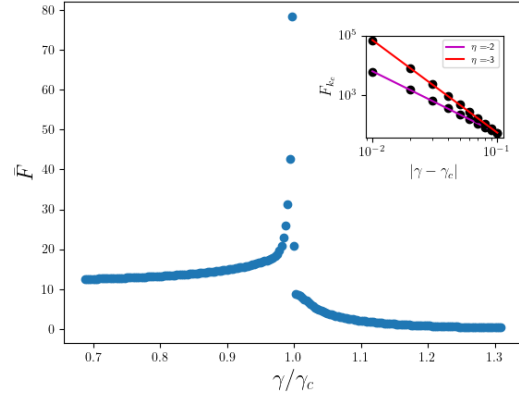


FIG. 3. The main figure illustrates the variation of the \bar{F} for different values of γ , where γ_c represents the critical value of the measurement rate ($h = 0.6$). In the inset, presented on a log-log plot, we depict the scaling behavior of the critical mode as reported in Eq. (22) ($F_{k_c} \propto 1/|\gamma - \gamma_c|^\eta$), in magenta the scaling for $\gamma < \gamma_c$ and in red for $\gamma > \gamma_c$.

a transverse magnetic field. Our analysis reveals a change in the scaling behaviour of the QFI across the transition point, with a super-extensive (sub-extensive) scaling law for values of the measuring rate γ below (above) its critical value $\gamma_c = \sqrt{h-1}$. This is revealed by the presence of multi-partite entanglement for $\gamma < \gamma_c$, not signalled for $\gamma > \gamma_c$. This behaviour is consistent with the entanglement phase transition observed through the entanglement entropy [4–6]. The QFI, however, provides a new insight into the multipartite nature of the entanglement associated with the two phases, demonstrating its usefulness as a resource for quantum metrology.

Additionally, we have shown that the MIPT can be revealed through the divergent behaviour of the QFI with respect to the measuring rate. This non-trivial finding parallels the analogous non-analyticity of the QFI across standard QPTs, when the QFI is evaluated with respect to the parameter driving the transition [22]. Our findings provide new insights into the behavior of quantum systems subjected to MIPT and highlight the potential use of MIPT for quantum technological purposes.

Future research should explore the impact of the MIPT on the QFI of other types of quantum systems and investigate the role of measurement in other physical quantities. These efforts will contribute to the development of quantum computing and metrology, and provide a deeper understanding of the behavior of quantum systems under measurement.

During the preparation of this manuscript the authors became aware of the related work [58], which analyses multipartite entanglement across MIPT.

-
- * giovanni.difresco01@unipa.it
† bernardo.spagnolo@unipa.it
‡ davide.valenti@unipa.it
§ angelo.carollo@unipa.it
- [1] D. Rossini and E. Vicari, Measurement-induced dynamics of many-body systems at quantum criticality, *Phys. Rev. B* **102**, 035119 (2020).
 - [2] X. Cao, A. Tilloy, and A. D. Luca, Entanglement in a fermion chain under continuous monitoring, *SciPost Phys.* **7**, 024 (2019).
 - [3] O. Alberton, M. Buchhold, and S. Diehl, Entanglement transition in a monitored free-fermion chain: From extended criticality to area law, *Phys. Rev. Lett.* **126**, 170602 (2021).
 - [4] A. Biella and M. Schiró, Many-body quantum Zeno effect and measurement-induced subradiance transition, *Quantum* **5**, 528 (2021).
 - [5] X. Turkeshi, A. Biella, R. Fazio, M. Dalmonte, and M. Schiró, Measurement-induced entanglement transitions in the quantum Ising chain: From infinite to zero clicks, *Phys. Rev. B* **103**, 224210 (2021).
 - [6] X. Turkeshi and M. Schiró, Entanglement and correlation spreading in non-Hermitian spin chains, *Phys. Rev. B* **107**, L020403 (2023).
 - [7] T. Minato, K. Sugimoto, T. Kuwahara, and K. Saito, Fate of measurement-induced phase transition in long-range interactions, *Phys. Rev. Lett.* **128**, 010603 (2022).
 - [8] M. J. Gullans and D. A. Huse, Dynamical purification phase transition induced by quantum measurements, *Phys. Rev. X* **10**, 041020 (2020).
 - [9] M. J. Gullans and D. A. Huse, Scalable probes of measurement-induced criticality, *Phys. Rev. Lett.* **125**, 070606 (2020).
 - [10] A. Chan, R. M. Nandkishore, M. Pretko, and G. Smith, Unitary-projective entanglement dynamics, *Phys. Rev. B* **99**, 224307 (2019).
 - [11] B. Skinner, J. Ruhman, and A. Nahum, Measurement-induced phase transitions in the dynamics of entanglement, *Phys. Rev. X* **9**, 031009 (2019).
 - [12] A. Nahum, S. Roy, B. Skinner, and J. Ruhman, Measurement and entanglement phase transitions in all-to-all quantum circuits, on quantum trees, and in Landau-Ginsburg theory, *PRX Quantum* **2**, 010352 (2021).
 - [13] S. Choi, Y. Bao, X.-L. Qi, and E. Altman, Quantum error correction in scrambling dynamics and measurement-induced phase transition, *Phys. Rev. Lett.* **125**, 030505 (2020).
 - [14] S. Sang, Y. Li, T. Zhou, X. Chen, T. H. Hsieh, and M. P. Fisher, Entanglement negativity at measurement-induced criticality, *PRX Quantum* **2**, 030313 (2021).
 - [15] A. Lavasani, Y. Alavirad, and M. Barkeshli, Measurement-induced topological entanglement transitions in symmetric random quantum circuits, *Nature Physics* **17**, 342 (2021).
 - [16] G. Mussardo, S. Navigation, and N. S. Route, *Statistical field theory : an introduction to exactly solved models in statistical physics* (Oxford University Press, 2010) p. 755.
 - [17] P. Zanardi, M. G. A. Paris, and L. Campos Venuti, Quantum criticality as a resource for quantum estimation, *Phys. Rev. A* **78**, 042105 (2008).
 - [18] C. Invernizzi, M. Korbman, L. Campos Venuti, and M. G. A. Paris, Optimal quantum estimation in spin systems at criticality, *Phys. Rev. A* **78**, 042106 (2008).
 - [19] M. Tsang, Quantum transition-edge detectors, *Phys. Rev. A* **88**, 021801 (2013).
 - [20] P. A. Ivanov and D. Porras, Adiabatic quantum metrology with strongly correlated quantum optical systems, *Phys. Rev. A* **88**, 023803 (2013).
 - [21] M. Bina, I. Amelio, and M. G. A. Paris, Dicke coupling by feasible local measurements at the superradiant quantum phase transition, *Phys. Rev. E* **93**, 052118 (2016).
 - [22] I. Frérot and T. Roscilde, Quantum critical metrology, *Phys. Rev. Lett.* **121**, 020402 (2018).
 - [23] T. L. Heugel, M. Biondi, O. Zilberberg, and R. Chitra, Quantum transducer using a parametric driven-dissipative phase transition, *Phys. Rev. Lett.* **123**, 173601 (2019).
 - [24] L. Garbe, M. Bina, A. Keller, M. G. A. Paris, and S. Felicetti, Critical quantum metrology with a finite-component quantum phase transition, *Phys. Rev. Lett.* **124**, 120504 (2020).
 - [25] P. A. Ivanov, Steady-state force sensing with single trapped ion, *Phys. Scr.* **95**, 025103 (2020).
 - [26] V. Montenegro, U. Mishra, and A. Bayat, Global sensing and its impact for quantum many-body probes with criticality, *Phys. Rev. Lett.* **126**, 200501 (2021).
 - [27] F. Albarelli and R. Demkowicz-Dobrzański, Probe incompatibility in multiparameter noisy quantum metrology, *Phys. Rev. X* **12**, 011039 (2022).
 - [28] R. Di Candia, F. Minganti, K. V. Petrovnin, G. S. Paraoanu, and S. Felicetti, Critical parametric quantum sensing 10.48550/ARXIV.2107.04503 (2021).
 - [29] G. D. Fresco, B. Spagnolo, D. Valenti, and A. Carollo, Multiparameter quantum critical metrology, *SciPost Phys.* **13**, 077 (2022).
 - [30] A. Carollo, D. Valenti, and B. Spagnolo, Geometry of quantum phase transitions, *Phys. Rep.* **838**, 1 (2020).
 - [31] P. Hyllus, W. Laskowski, R. Krischek, C. Schwemmer, W. Wieczorek, H. Weinfurter, L. Pezzé, and A. Smerzi, Fisher information and multiparticle entanglement, *Phys. Rev. A* **85**, 022321 (2012).
 - [32] G. Tóth, Multipartite entanglement and high-precision metrology, *Phys. Rev. A* **85**, 022322 (2012).
 - [33] H. Strobel, W. Muessel, D. Linnemann, T. Zibold, D. B. Hume, L. Pezzé, A. Smerzi, and M. K. Oberthaler, Fisher information and entanglement of non-gaussian spin states, *Science* **345**, 424 (2014).
 - [34] P. Hauke, M. Heyl, L. Tagliacozzo, and P. Zoller, Measuring multipartite entanglement through dynamic susceptibilities, *Nat. Phys.* **12**, 778 (2016), 1509.01739.
 - [35] C. W. Helstrom, *Quantum detection and estimation theory* (Academic Press, 1976).
 - [36] M. Szczykulska, T. Baumgratz, and A. Datta, Multiparameter quantum metrology, *Adv. Phys. X* **1**, 621 (2016).
 - [37] F. Albarelli, M. Barbieri, M. Genoni, and I. Gianani, A perspective on multiparameter quantum metrology: From theoretical tools to applications in quantum imaging, *Phys. Lett. A* **384**, 126311 (2020).
 - [38] M. A. Ballester, Entanglement is not very useful for estimating multiple phases, *Phys. Rev. A* **70**, 032310 (2004).
 - [39] C. Vaneph, T. Tufarelli, and M. G. Genoni, Quantum estimation of a two-phase spin rotation, *Quantum Meas. Quantum Metrol.* **1**, 12 (2013).
 - [40] M. G. Genoni, M. G. A. Paris, G. Adesso, H. Nha, P. L.

- Knight, and M. S. Kim, Optimal estimation of joint parameters in phase space, *Phys. Rev. A* **87**, 012107 (2013).
- [41] H. Yuan and C.-H. F. Fung, Optimal feedback scheme and universal time scaling for Hamiltonian parameter estimation, *Phys. Rev. Lett.* **115**, 110401 (2015).
- [42] D. W. Berry, M. Tsang, M. J. W. Hall, and H. M. Wiseman, Quantum Bell-Ziv-Zakai bounds and Heisenberg limits for waveform estimation, *Phys. Rev. X* **5**, 031018 (2015).
- [43] M. Gessner, L. Pezzè, and A. Smerzi, Sensitivity bounds for multiparameter quantum metrology, *Phys. Rev. Lett.* **121**, 130503 (2018).
- [44] J. Rubio and J. Dunningham, Bayesian multiparameter quantum metrology with limited data, *Phys. Rev. A* **101**, 032114 (2020).
- [45] A. Carollo, B. Spagnolo, A. A. Dubkov, and D. Valenti, On quantumness in multi-parameter quantum estimation, *J. Stat. Mech. Theory Exp.* **2019**, 094010 (2019).
- [46] F. Albarelli, J. F. Friel, and A. Datta, Evaluating the Holevo Cramér-Rao bound for multiparameter quantum metrology, *Phys. Rev. Lett.* **123**, 200503 (2019).
- [47] J. S. Sidhu, Y. Ouyang, E. T. Campbell, and P. Kok, Tight bounds on the simultaneous estimation of incompatible parameters, *Phys. Rev. X* **11**, 011028 (2021).
- [48] M. Tsang, F. Albarelli, and A. Datta, Quantum semi-parametric estimation, *Phys. Rev. X* **10**, 031023 (2020).
- [49] R. Demkowicz-Dobrzański, W. Górecki, and M. Guţă, Multi-parameter estimation beyond quantum Fisher information, *J. Phys. A Math. Theor.* **53**, 363001 (2020).
- [50] E. H. Lieb, T. Schultz, and D. Mattis, Two soluble models of an antiferromagnetic chain, *Ann. Phys. (N. Y.)* **16**, 407 (1961).
- [51] E. Barouch and B. M. McCoy, Statistical mechanics of the XY model. II. Spin-correlation functions, *Phys. Rev. A* **3**, 786 (1971).
- [52] G. B. Mbeng, A. Russomanno, and G. E. Santoro, The quantum Ising chain for beginners (2020).
- [53] T. E. Lee and C.-K. Chan, Heralded magnetism in non-Hermitian atomic systems, *Phys. Rev. X* **4**, 041001 (2014).
- [54] We have also explored different directions, but our results indicate that the x-direction is the most compelling.
- [55] S. Ragy, M. Jarzyna, and R. Demkowicz-Dobrzański, Compatibility in multiparameter quantum metrology, *Phys. Rev. A* **94**, 052108 (2016).
- [56] M. Skotiniotis, P. Sekatski, and W. Dür, Quantum metrology for the Ising Hamiltonian with transverse magnetic field, *New Journal of Physics* **17**, 073032 (2015).
- [57] Strictly speaking, there is a minor misuse of notation. In the case of $\gamma < \gamma_c$, the critical mode k_c has a real eigenvalue ϵ_{k_c} , resulting in a time dependence which is not exponential, but proportional to t^2 . However, a careful analysis of this case does not impact the bounds in Eq.(21). This behaviour is indeed taken into account explicitly in our examination of the critical mode's scaling.
- [58] A. Paviglianiti and A. Silva, Multipartite entanglement in the measurement-induced phase transition of the quantum Ising chain (2023).
- [59] R. R. Puri, Algebra of the exponential operator, in *Mathematical Methods of Quantum Optics* (Springer Berlin Heidelberg, Berlin, Heidelberg, 2001) pp. 37–53.

Appendix A

To ensure clarity and self-consistency, in this Appendix we provide a set of information and details of the non-Hermitian Hamiltonian in Eq. (3). Firstly, we employ the Jordan-Wigner transformation

$$\begin{cases} \sigma_i^x = \prod_{j<i} (2n_j - 1) (c_i + c_i^\dagger) \\ \sigma_i^z = 1 - 2c_i^\dagger c_i \end{cases} \quad (23)$$

to rewrite our Hamiltonian in fermionic language. Subsequently, we move to the momentum space through the Fourier transform $c_j = \frac{e^{i\pi/4}}{\sqrt{N}} \sum_k e^{ikj} c_k$. This results in the expression of Eq. (4)

$$H = \sum_k (c_k^\dagger \ c_{-k}) M_k \begin{pmatrix} c_k \\ c_{-k}^\dagger \end{pmatrix}, \quad (24)$$

where

$$M_k = \begin{pmatrix} \alpha_k & \beta_k \\ \beta_k & -\alpha_k \end{pmatrix}. \quad (25)$$

In this work, every time we considered the expression of the Hamiltonian in the momentum space, we worked with periodic boundary conditions on the spin chain and an even number of fermions. This corresponded to use anti-periodic boundary conditions for the fermionic chain with

$$k = \left\{ \frac{(2n-1)\pi}{N} \mid n = 1, \dots, \frac{L}{2} \right\}, \quad (26)$$

where only the positive values were used due to the symmetries of the Hamiltonian. We also note that in Eq. (4), a constant term was neglected as it does not affect the system's dynamics. The eigenvalues of Eq.(25), denoted as $\epsilon_k = \pm \sqrt{\epsilon_k^2 + \Delta_k^2}$, possess both real and imaginary parts. The real and imaginary parts are denoted as $E_k = \Re(\epsilon_k)$ and $\Gamma_k = \Im(\epsilon_k)$, respectively. It is important to note that the convention on the sign can be chosen independently for each k in the system's spectrum. In this study, we have chosen the convention such that $\Gamma_k \leq 0$ always. Furthermore, it is worth noting that there exists a critical value of k , given by $k_c = \arccos(-h)$, where ϵ_k is real for $\gamma \leq \gamma_c$ and imaginary for $\gamma > \gamma_c$. This peculiar behavior of non-Hermitian systems is illustrated in Fig.4, where the behavior of the spectrum is reported for various values of γ .

The time-dependent state can be computed easily due to the initial state's well-defined parity and translation invariance. As a result, the dynamics can be decomposed into $N/2$ independent ones

$$|\psi\rangle = \prod_k |\psi_k\rangle. \quad (27)$$

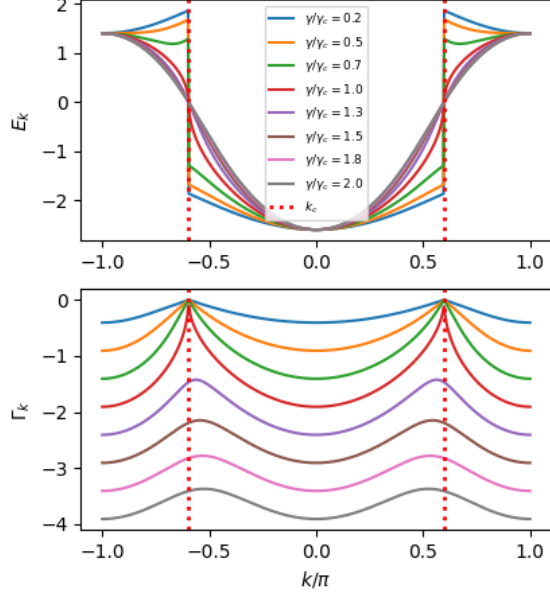


FIG. 4. The figure presents the spectrum of the Hamiltonian in Eq. (4) for different values of the measurement rate γ . The upper panel displays the real part of the spectrum, gapped at $\pm k_c$ for $\gamma/\gamma_c < 1$, while it becomes gapless for $\gamma/\gamma_c \geq 1$. On the other hand, the lower panel shows the behavior of the imaginary part, which attains its maximum value $\Gamma = 0$ at $\pm k_c$ for $\gamma \leq \gamma_c$, whereas it remains non-zero for $\gamma > \gamma_c$.

If we denote with $|\tilde{\psi}\rangle = (u_k + v_k c_k^\dagger c_{-k}^\dagger)|0\rangle$ the unnormalized k state we can easily see that its dynamics is given by

$$i \frac{d}{dt} \begin{pmatrix} u_k \\ v_k \end{pmatrix} = M_k \begin{pmatrix} u_k \\ v_k \end{pmatrix} \quad (28)$$

whose solution is given in Eq. (19).

Appendix B

This Appendix presents the derivation of the QFI expression for the non-Hermitian quantum quench. As mentioned in the main text, the state at time t can be expressed as a function of the initial state $|\psi_0\rangle$, using the general form

$$|\psi(t)\rangle = N(t) e^{-iH_{\text{eff}}t} |\psi_0\rangle. \quad (29)$$

To obtain the QFI, it is necessary to compute the derivative of the state with respect to a parameter of interest, which can be expressed as

$$|\partial_\lambda \psi\rangle = \left(\partial_\lambda N(t) e^{-iH_{\text{eff}}t} + N(t) \partial_\lambda e^{-iH_{\text{eff}}t} \right) |\psi_0\rangle. \quad (30)$$

It is important to note that the derivative of the exponential term in the last term of Eq. (30) should be carefully

considered, as $\partial_\lambda H$ and H do not commute. By using *Sneddon's formula* [59] allows us to express Eq. (30) as

$$\begin{aligned} |\partial_\lambda \psi\rangle &= \left(\frac{\partial_\lambda N(t)}{N(t)} + \int_0^t ds \exp(-iH_{\text{eff}}s) \partial_\lambda (-iH_{\text{eff}}) \exp(iH_{\text{eff}}s) \right) |\psi\rangle = \\ &= \left(\frac{\partial_\lambda N(t)}{N(t)} + \hat{O}_\lambda \right) |\psi\rangle, \end{aligned} \quad (31)$$

and applying the general definition of the QFI, we can easily obtain

$$\begin{aligned} \frac{F}{4} &= \left(\langle \partial_\lambda \psi | \partial_\lambda \psi \rangle - |\langle \partial_\lambda \psi | \psi \rangle|^2 \right) = \\ &= \left(\langle \psi | \left(\left(\frac{\partial_\lambda N}{N} \right)^* + O_\lambda^\dagger \right) \left(\frac{\partial_\lambda N}{N} + O_\lambda \right) | \psi \rangle \right) \\ &\quad - \left(\frac{\partial_\lambda N}{N} + \langle \psi | O_\lambda | \psi \rangle \right) \left(\left(\frac{\partial_\lambda N}{N} \right)^* + \langle \psi | O_\lambda^\dagger | \psi \rangle \right) = \\ &= \langle \psi | O_\lambda^\dagger O_\lambda | \psi \rangle - \langle \psi | O_\lambda | \psi \rangle \langle \psi | O_\lambda^\dagger | \psi \rangle. \end{aligned} \quad (32)$$

The closed expression for the operator O_γ in Eq. (17) can be obtained by explicitly computing the derivative of the Hamiltonian with respect to γ , which yields the following result

$$\begin{aligned} O_\gamma &= - \int_0^t ds e^{-iH_{\text{eff}}s} \sum_k (c_k^\dagger \ c_{-k}) \begin{pmatrix} 1 & 0 \\ 0 & -1 \end{pmatrix} \begin{pmatrix} c_k \\ c_{-k}^\dagger \end{pmatrix} e^{iH_{\text{eff}}s} \\ &\quad - \frac{Nt}{4}. \end{aligned} \quad (33)$$

After evaluating the equation of motion for the operator c_k we can rewrite Eq. (33) as

$$\begin{aligned} O_\gamma &= \sum_k (c_k^\dagger \ c_{-k}) \left[\int_0^t ds e^{-iM_k s} \begin{pmatrix} 1 & 0 \\ 0 & -1 \end{pmatrix} e^{iM_k s} \right] \\ &\quad \begin{pmatrix} c_k \\ c_{-k}^\dagger \end{pmatrix} - \frac{Nt}{4}. \end{aligned} \quad (34)$$

At this point, following a series of tedious but straightforward algebraic manipulations, we arrive at the conclusion that

$$O_\gamma = - \sum_k (c_k^\dagger \ c_{-k}) R_k \begin{pmatrix} c_k \\ c_{-k}^\dagger \end{pmatrix} - \frac{Nt}{4}, \quad (35)$$

where

$$\begin{aligned} R_k &= \begin{pmatrix} A_k & B_k \\ C_k & -A_k \end{pmatrix} = \\ &= \begin{pmatrix} \frac{t\alpha_k^2}{\epsilon_k^2} + \frac{\sin(2\epsilon_k t)}{2\epsilon_k^3} \beta_k^2 & \frac{\alpha_k \beta_k t}{\epsilon_k^2} + \frac{2\beta_k \sin^2(\epsilon_k t) \epsilon_k i - \alpha_k \beta_k \sin(2\epsilon_k t)}{2\epsilon_k^3} \\ \frac{\alpha_k \beta_k t}{\epsilon_k^2} - \frac{2\beta_k \sin^2(\epsilon_k t) \epsilon_k i + \alpha_k \beta_k \sin(2\epsilon_k t)}{2\epsilon_k^3} & -\frac{t\alpha_k^2}{\epsilon_k^2} - \frac{\sin(2\epsilon_k t)}{2\epsilon_k^3} \beta_k^2 \end{pmatrix} \end{aligned} \quad (36)$$

Using the expression of Eq.(18), we can evaluate the expectation value of Eq.(32), resulting in the following ex-

pression

$$\begin{aligned} \frac{F}{4} &= \langle \psi | O_\lambda^\dagger O_\lambda | \psi \rangle - \langle \psi | O_\lambda | \psi \rangle \langle \psi | O_\lambda^\dagger | \psi \rangle = \\ &= \sum_k \left[\frac{[|u_k|^2 (|A_k|^2 + |C_k|^2) - 2\Re(u_k^* v_k (-A_k B_k^* + C_k A_k^*)) + |v_k|^2 (|A_k|^2 + |B_k|^2)]}{|u_k|^2 + |v_k|^2} \right. \\ &\quad \left. - \left| \frac{(-|u_k^2 A_k - C_k u_k^* v_k - B_k u_k v_k^* + A_k |v_k|^2)}{|u_k|^2 + |v_k|^2} \right|^2 \right]. \end{aligned} \quad (37)$$

When examining the long-time behavior of the QFI, it becomes evident that we can factorize the exponential scaling. This can be seen from

$$\begin{cases} A_k = \pm \frac{i\beta_k^2}{4\epsilon_k^3} e^{2i\tilde{\epsilon}_k} = \tilde{A}_k e^{2i\tilde{\epsilon}_k} \\ B_k = i \frac{-\beta_k \epsilon_k \mp \alpha_k \beta_k}{4\epsilon_k^3} e^{2i\tilde{\epsilon}_k} = \tilde{B}_k e^{2i\tilde{\epsilon}_k} \\ C_k = i \frac{\beta_k \epsilon_k \mp \alpha_k \beta_k}{4\epsilon_k^3} e^{2i\tilde{\epsilon}_k} = \tilde{C}_k e^{2i\tilde{\epsilon}_k} \end{cases} \quad (38)$$

where $\tilde{\epsilon}_k$ is the eigenvalue with positive imaginary part (these scaling laws are valid for all values of k and γ , ex-

cept for k_c when $\gamma < \gamma_c$). To compute the long time behavior of the QFI we can evaluate the expectation value using the ground state of the effective Hamiltonian [53]. Then follows that the long time behavior of the quantum Fisher information is

$$\begin{aligned} F &= \sum_k \left[\frac{(|\tilde{u}_k|^2 (|\tilde{A}_k|^2 + |\tilde{C}_k|^2) - 2\Re(\tilde{u}_k \tilde{v}_k^* (\tilde{A}_k^* \tilde{C}_k - \tilde{A}_k \tilde{B}_k^*)) + |\tilde{v}_k|^2 (|\tilde{A}_k|^2 + |\tilde{B}_k|^2))}{(|\tilde{u}_k|^2 + |\tilde{v}_k|^2)} e^{4\Gamma_k t} \right. \\ &\quad \left. - \frac{[(-\tilde{A}_k |\tilde{u}_k|^2 - \tilde{C}_k \tilde{u}_k^* \tilde{v}_k - \tilde{B}_k \tilde{u}_k \tilde{v}_k^* + \tilde{A}_k |\tilde{v}_k|^2)]^2 e^{4\Gamma_k t}}{(|\tilde{u}_k|^2 + |\tilde{v}_k|^2)^2} \right] = \\ &= \sum_k F_k e^{4\Gamma_k t}. \end{aligned} \quad (39)$$

The critical mode's expression of the QFI can be determined analytically by assessing Eq.(39) for $k_c = \arccos(-h)$. When $\gamma > \gamma_c$, the QFI can be computed using the expressions provided in Eq.(38). In contrast, when $\gamma < \gamma_c$, the linear term in t becomes the leading term in the long time approximation of Eq. (36). This phenomenon is responsible for the difference in the scaling laws of Eq. (22).